AE4135 Rotor / wake Aerodynamics

Assignment 1

by

Peter Blom 4475011
Jur Mijjer 4459210
Olaf Nekeman 4367642

Professor: Prof. Dr. Ir. Carlos Simão Ferreira
Dr. ir. Tomas Sinnige

Contents

List of Figures

List of Tables

1
Lifting-line Method

1.1. Introduction

For this assignment the lifting-line method is used to analyse the performance of a wind turbine and propeller. In the previous assignment, an optimised geometry is found for both corresponding to a maximum power coefficient for a thrust coefficient equal to 0.75. An overview of the parameters of the wind turbine and propeller can be found in Table 1.1. Additionally, the operations conditions used for the analysis are specified in Table 1.2. Note, as presented in the previous assignment there was no optimised geometry determined for a TSR equal to 6 and thus this tip speed ratio has not been included in the analysis.

Table 1.1: Parameters used for the analysis. Custom means that the distribution is described with a vector, one value per radial position.

Parameters	**Wind turbine**	**Propeller**
Amount of blades N_{blades}	3	6
Radius R	50 m	0.7 m
Blade starting location	0.2 r/R	0.25 r/R
Twist distribution	$-10.84 + 15.58 \cdot$(r/R) ° for a TSR = 8 $-7.64 + 12.85 \cdot$(r/R) ° for a TSR = 10	Custom
Chord distribution	$4.47 - 3.70 \cdot$(r/R) m for a TSR = 8 $2.94 - 2.44 \cdot$(r/R) m for a TSR = 10	Custom

Table 1.2: Operating conditions used for the analysis

Condition	**Wind turbine**	**Propeller**
U_∞	10 m/s	60 m/s
TSR	8, 10	1.47
RPM	15.28, 19.10.	1200
ISA altitude	2000 m	2000 m

The above presented parameters will be used as inputs for the lifting-line method in order to analyse the performance of the two rotors, similarly as done for the Blade Element Momentum theory (BEM) in the previous assignment. The result of this analysis for the wind turbine and the propeller can be found in Chapter 3 and Chapter 4 respectively. Additionally, the effect of changing input parameters such as the spacing of the blade elements on the model output result will be examined. The method with its assumption and the Python program that is developed for this analysis will be presented in the following sections of this chapter. Moreover, the effect of two wind turbine rotors side-by-side on the performance will be analysed and presented in Chapter 5.

1.2. Main Model Assumptions

In this section the main assumptions used for the application of the lifting-line method will be discussed. Firstly, the model is developed for an horizontal axis wind turbine and propeller which both encounter a steady, uniform and axial inflow. On top of that, similarly as to the previous assignment, the flow is considered to be incompressible and inviscid. Moreover, it defines the blade and the wake of the blade as a sum of elements, where for the wake a frozen wake geometry is assumed.

The lifting-line method is used for preliminary calculations of characteristics of a wing or rotor blade. It models the generated lift by vortex filaments that are position at 1/4 chord location of the blade, corresponding to the bound vortex. Using Helmholtz's second theorem that a vortex filament does not end in fluid[1], two trailing vortices are generated at the tip and start of the blade, which moves downstream to infinity. Thus, resulting in a horseshoe vortex. For the lifting-line theory the blade is modeled with a number of blade elements which all have a bound vortex at 1/4 chord location and a horseshoe vortex.

Additionally, the wake is modelled as a frozen wake vortex model. This modelling assumes that the wake is solely dependent on the geometric boundary conditions and the unperturbed inflow. Hence, this includes that it assumed that the wake is not deformed and velocity difference induced by the blades is neglected[2]. This will have an effect on the results as the wake geometry determined the induction at the bound vortex. Furthermore, vortex cores are used in order to model the viscous effects of the wake and hence the induced velocity by the wake. Lastly, the wake is modelled as a finite wake instead of an infinite wake as the sensitivity analysis showed that after a certain finite wake length the power and thrust coefficient converges.

1.3. Model description

The flowchart of the code can be found in Figure 1.1 to Figure 1.2. The former shows that with the airfoil polar as input the rotor blades will be modelled using the lifting line theory. Furthermore, Figure 1.3 shows the part of the code corresponding to solving the system defined as shown in Figure 1.1. This will actually output the circulation, axial force, azimuthal force and subsequently the thrust and power coefficient obtained by using the lifting line theory. The entire code will be handed in with the assignment.

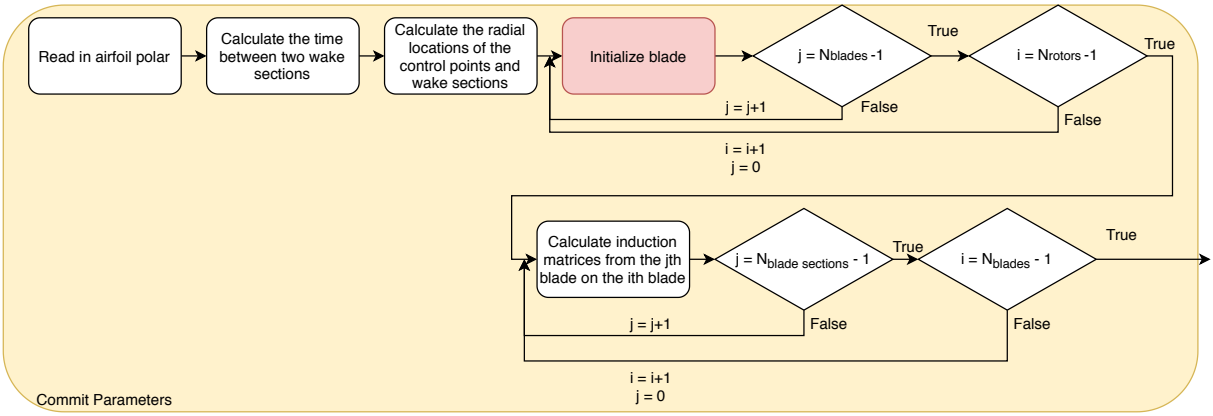

Figure 1.1: Flowchart of the code which is executed when the user calls the function *commit_parameters* from the class *lifting_line_model* or *lifting_line_model_singular*. Note that the flowchart in the red block can be found in Figure 1.2.

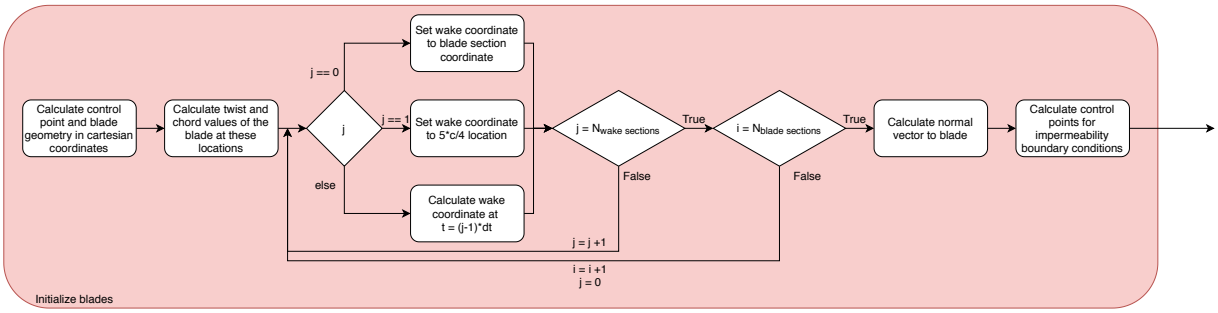

Figure 1.2: Flowchart of the code which is executed when the class *blade* is initialized.

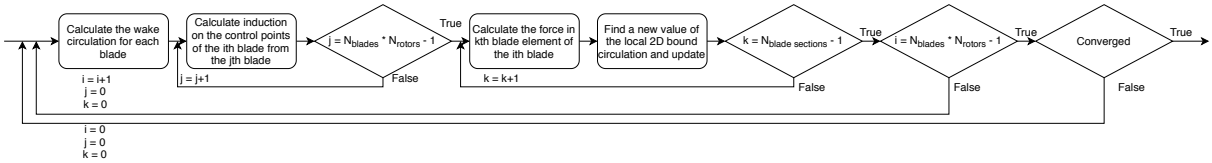

Figure 1.3: Flowchart of the code which is executed when the user calls the function *solve_system* from the class *lifting_line_model* or *lifting_line_model_singular*.

The results obtained by the code will be non-dimensionalised in order to obtain coefficients that represent the parameters. This is valuable as it gives the possibility to do experiments in the future to validate the models used for these assignment. This gives the opportunity to compare the results of the analysis with a scaled wind tunnel test of the turbine or rotor. The forces will be non-dimensionalized by dividing by $\frac{1}{2}\rho U_\infty^2 R$ and the circulation by dividing by $(U_\infty^2 \pi)/(N_{blades}\Omega)$.

2
Sensitivity Analysis

The sensitivity analysis was conducted on the four main variables in the system: type of spatial discretization, wake convection speed, azimuthal discretization and the length of the wake. Each parameter is discussed in its own paragraph, with an explanation of the setup of the experiment, followed by the results of the analysis. Every paragraph closes with a discussion of the relative impact of the parameter on the lifting line model. The general parameters used in the sensitivity analysis are given in table 2.1. In each experiment, one of these parameters is evaluated.

Table 2.1: General parameter settings for the sensitivity analysis.

Variable	Value
Spacing	'cosine'
N blade sections	50
N wake sections	30
N rotations	16
Wake velocity	7.31 m/s
Vortex core size	0.02
TSR	8

2.1. Effect of wake convection speed

The wake convection speed is determined by equation 2.1 and depends on the wake induction factor a_w. Thus, these terms can be used interchangably. The effect of the wake induction factor is large. In the BEM analysis, it was one of the main parameters affecting the rotor performance. In the lifting line, it also affects the performance but in a different way. Here the blade geometry is fixed and we try to find the right wake induction factor to use for further analysis. In order to compare a BEM and lifting line model, the C_T values have to be equal for both. Therefore, a convergence loop was written and can be recognized by the asterisk (*) in the results.

The results are shown in figure 2.1. What can be derived from this figure is that the convection speed of the wake strongly influences the circulation on the blade, and thus the performance of the rotor. The results for C_T=0.75 is a_{wake}=0.269. Furthermore, the $a_{wake}*$ gives a C_P=0.4822. This is very close to the BEM result of C_P=0.4783. The comparison between the BEM and lifting is further explained in section 3.2. The main takeaway is that the proper wake induction factor is found through this analysis.

Table 2.2: Results for difference wake velocities in the lifting line model. * Result from loop which converges to C_T=0.75.

Convection velocity (m/s)	a_w	C_T	C_P	**Execution time (s)**
9.0	0.1	0.7767	0.5276	102
7.31*	0.269	0.7500	0.4822	N/A
7.0	0.3	0.7435	0.4720	104
5.0	0.5	0.6869	0.3864	102
3.0	0.7	0.5812	0.2497	106

$$U_{wake} = U_\infty \cdot (1 - a_w) \tag{2.1}$$

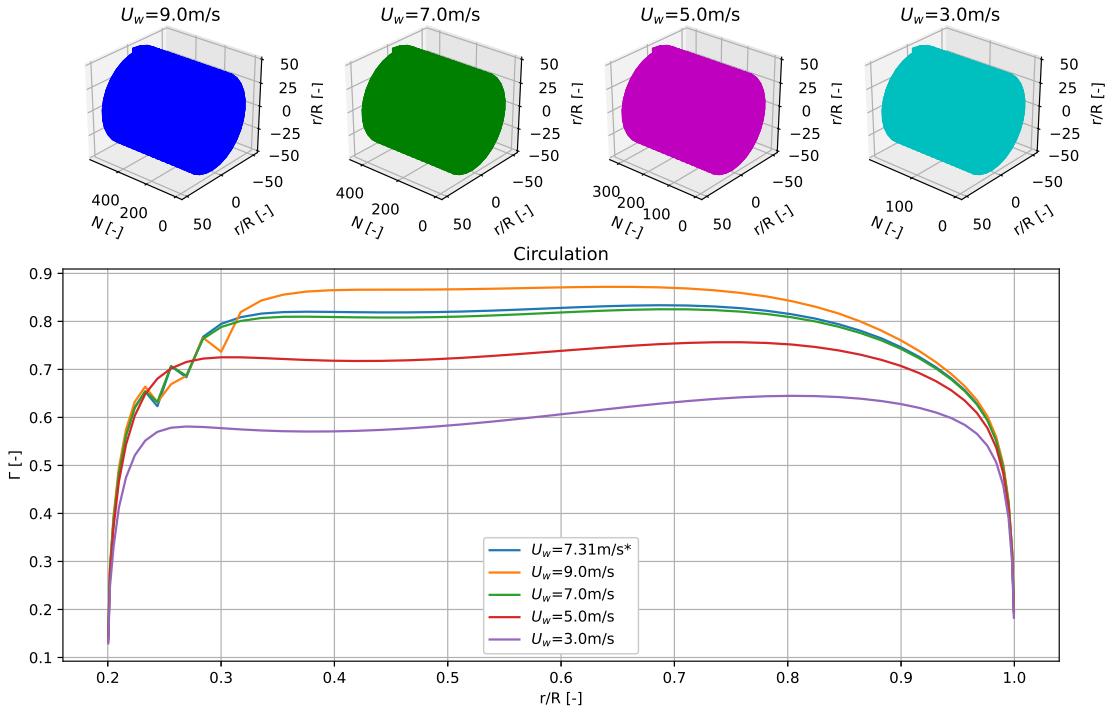

Figure 2.1: Geometry and induction factors for a lifting line model with different wake lengths.

2.2. Type of spatial discretization

There are two types of spatial discretization used for the lifting line model: uniform spacing or cosine spacing. The uniform spacing method means that the blade is discretization in sections of equal length. This means that the distribution of points for evaluation is uniform. In cosine spacing, the blade is split up in equal lengths along a semi-circle. This is shown in figure 2.2. This creates a denser coverage of sections at the tip and root of blade and reduces the coverage in the middle sections, compared to the uniform method. This could be beneficial because the gradients of the force and circulation are larger at the tip and root, thus requiring a higher resolution to describe the behavior as precise as possible. For the analysis, both methods were ran.

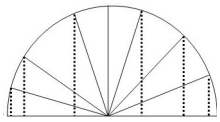

Figure 2.2: Cosine spacing method example.

What can be derived from figure 2.3 is that the cosine method is preferred over the uniform spacing. There are three reasons for this. Firstly, the cosine method represents the places where the change in gradient is the largest the best. This is near the root and the tip of the blade. A blade experience root and tip vortices, which influence the performance of the system. These effects results in large changes of the gradient of circulation near those point, thus require a high resolution. Furthermore, in the middle sections, the cosine and uniform spacing method show little difference in circulation. With this knowledge, the next experiments will use the cosine spacing method.

Table 2.3: Results for the real, uniform and cosine discretization of the blade sections.

Type	Ct	Cp	Execution time (s)
Uniform	0.7524	0.4849	98
Cosine	0.7500	0.4822	118

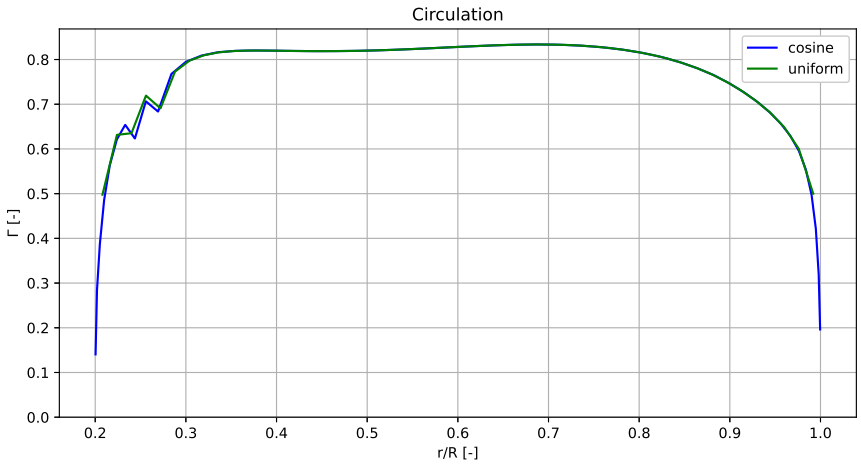

Figure 2.3: Circulation for a blade concerning the two types of spatial discretization methods: uniform and cosine.

2.3. Number of blade sections

The number of blade sections impact the overall resolution of the system. One mayor disadvantage with increasing the number of blade sections is the additional computational effort it requires. Therefore, it is a trade between speed and accuracy. However, too many blade sections might result in an unstable system. These effects are studied in this experiment.

Figure 2.4 shows the results of the experiment. What can be derived from this is that the line smoothes as the resolution increases, up to 20 segments. After this, it appears that the result fluctuates a lot near the tip and the root of the blade. The reason for this effect was found in the viscous core size, used in the program. An extra analysis for varying core size executed and explained in section 2.4. From this paragraph, it was found that the viscous core size should be below 0.1 for a smooth curve.
Secondly, the execution time increases with the resolution, as expected. It appears to scale quadratic.

Table 2.4: Results for different number of blade section for the blade discretization.

N blade sections	Ct	Cp	Execution time (s)
5	0.7640	0.5020	1.39
10	0.7561	0.4907	8.07
20	0.7526	0.4855	23.0
50	0.7500	0.4817	118

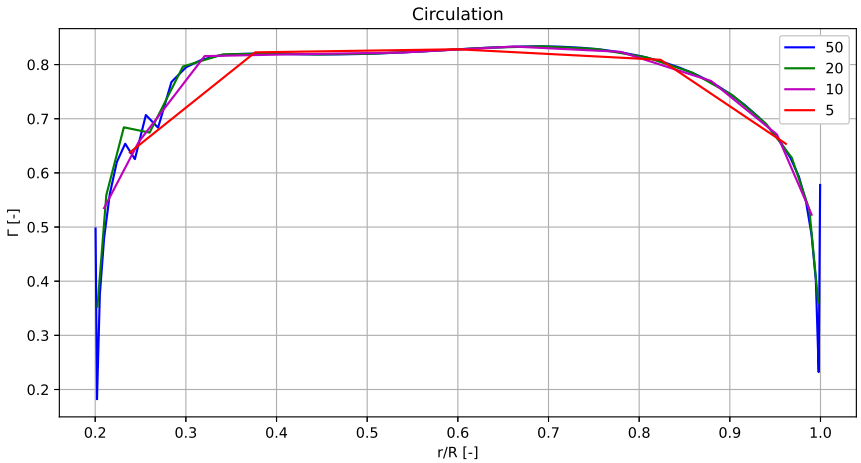

Figure 2.4: Circulation of a blade in the lifting line model with different number of blade sections.

2.4. Effect of viscous core size

The size of the viscous core has an effect on the stability of the system for large number of blade sections, as was shown in figure 2.4. In this paragraph, the maximum core size which still results in a stable curve is found.
The general results in table 2.5 show that for values below the 0.2, the C_T and C_P values vary little. Therefore, from the general results, an optimum value cannot be found. Thus, the optimum value was found by analyzing the root and tip sections in the circulation plots in figure 2.5. The root of the blade is shown in figure 2.5b. In this plot, the smoothest curve is chosen to be the best fit for the analysis. In this figure, the core size = 0.02 has the most constant results. Therefore, we have chosen to set the core size at 0.02 for further analysis.

Table 2.5: Results for different viscous core sizes.

Viscous core size	Ct	Cp
0.5	0.7517	0.4831
0.2	0.7502	0.4811
0.1	0.7488	0.4803
0.05	0.7499	0.4815
0.02	0.7491	0.4808
0.01	0.7491	0.4808

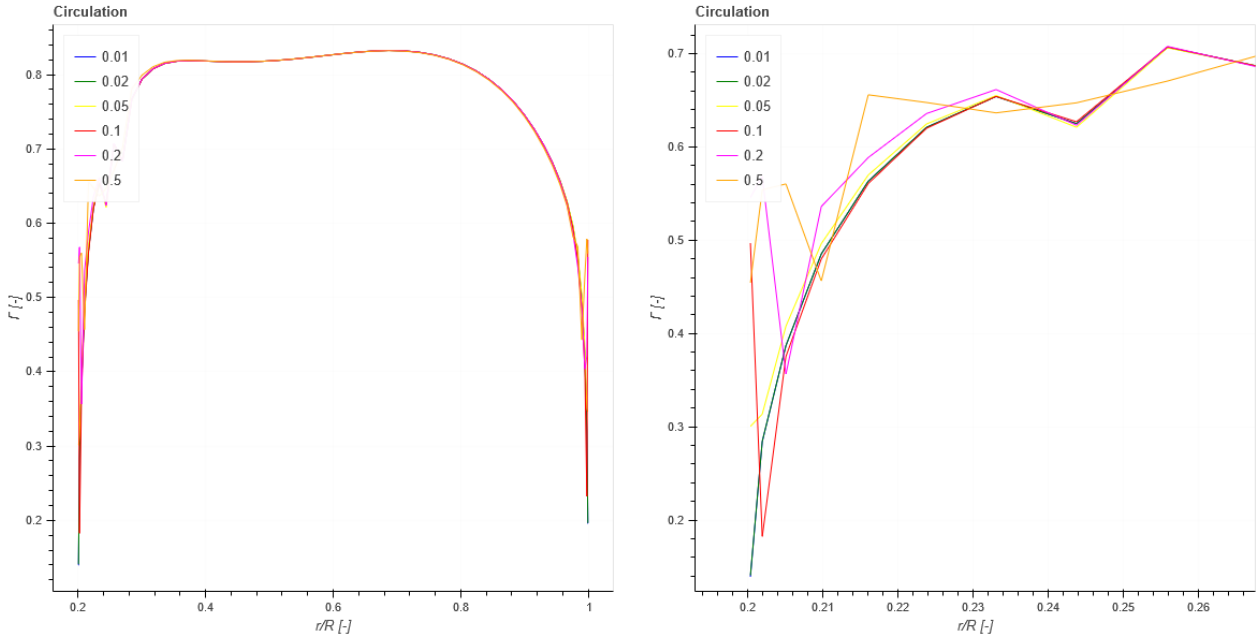

(a) Overall result.

(b) Close up of the root.

Figure 2.5: Sensitivity analysis for the viscous core size.

2.5. Length of the wake

The length of the wake is determined through the number of rotations of the blade in the analysis. It influences the development of the wake. The effect of the wake length is evaluated on its effect on the induction factor. This gives better insight in the development of the wake.

The thrust and power coefficient and the execution time per setting is given in table 2.6. The result shows that the execution scales linearly with the wake length. This is logical as the number of calculations is dependent on the number of nodes, which increases linearly with the wake length. Secondly, thrust and force coefficient are inversely proportional with the wake length. This says that as the wake develops more, the effect on the thrust and power of the rotor declines. Also, because the the execution time scales linearly and the C_T and C_P scale inversely proportional, there is a trade off but also an optimum wake length. For the purpose and feasibility of this assignment, it was decided to set the wake length at $N_{rotations} = 16$. This is confirmed by figure 2.6, where the curve of $N_{rotations} = 16$ is on the same curve for $N_{rotation} = 100$, which represents an infinite wake length in this analysis.

Table 2.6: Results for different number of blade section for the blade discretization.

N rotations	Ct	Cp	Execution time (s)
2	0.7762	0.5278	18.2
4	0.7595	0.4983	30.4
8	0.7523	0.48603	56.6
16	0.7500	0.4822	103
32	0.7494	0.4812	202
100	0.7492	0.4809	627

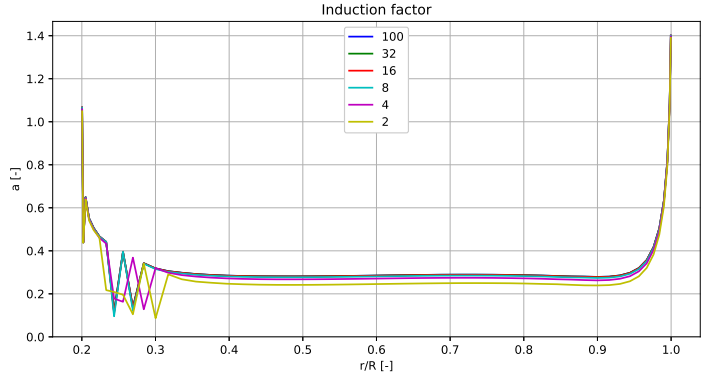

(a) Overall result.

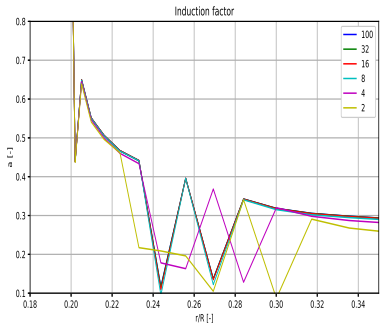

(b) Close up of the root.

Figure 2.6: Induction factors for a lifting line model with different wake lengths.

3
Wind Turbine

In this chapter the performance of the presented wind turbine will be analysed using the Lifting-line theory. First, the model and the analysis will be briefly discussed in Section 3.1. Afterwards, the results of the analysis will be presented in Section 3.2.

3.1. Model

Using the lifting line theory and the assumption of a frozen wake makes it able to estimate the wake of the turbine. An simulation has been done for the turbine with the parameters shown in Table 3.1. The wake convection induction factor expressed in the table is used in order to compute the convection speed of the frozen wake. This computation is done with Equation 2.1.

Parameter	Value
Number of blade sections	50
Number of wake sections	50
Number of rotations of the rotor	16
Wake convection induction factor a_{wake}	0.276 for TSR = 8 0.281 for TSR = 10
Vortex core size	0.02

Table 3.1: Parameters used for the lifting line model simulation.

The above presented parameters are used to estimate the wake of the turbine and are chosen using the result of the sensitivity analysis. An example of a lower number of rotations (equal to 5) and a TSR equal to 8 can be observed in Figure 3.1. It shows the three wakes that are created by the three blades of the turbine with the same convection difference between the three blades. Moreover, the wake for one blade of the geometry can be observed in Figure 3.2, where Figure 3.2a corresponds to a TSR of 8 and Figure 3.2b corresponds to a TSR of 10. For the different tip speed ratios it can be observed that the lower tip speed ratio results in a larger convection of the wake as shown on the axis.

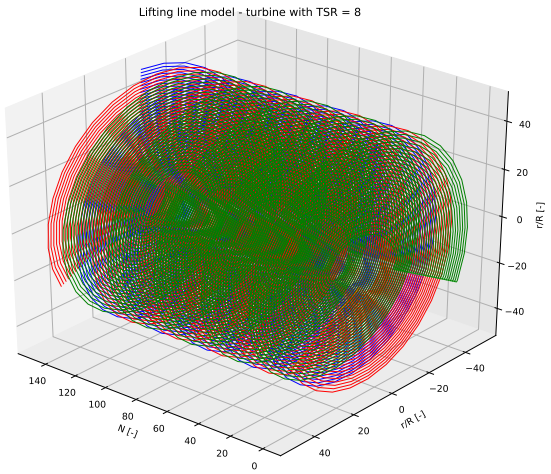

Figure 3.1: Visual representation of the wake of the turbine.

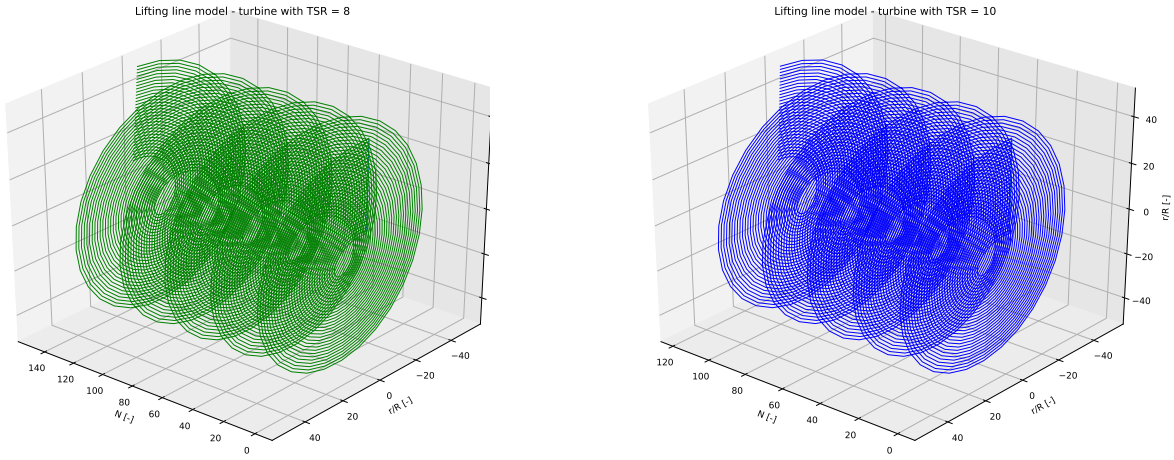

(a) TSR = 8

(b) TSR = 10

Figure 3.2: Visual representation of the wake of one of the blades of the turbine.

3.2. Simulation results

The results obtained with the lifting line theory will be discussed in this section. First, the power and thrust coefficients will be presented and afterwards the other performance parameters will be presented. Both the results will also be compared to the results that were obtained by the Blade Element Momentum theory (BEM).

3.2.1. Thrust and power coefficient

The coefficients obtained by the model are presented in Table 3.2. It can be seen that with a similar thrust coefficient for both TSR the power coefficient is estimated to be larger than was done for BEM. Moreover, it can be seen that the geometry designed for a TSR equal to 8 results in a higher power coefficient than for the geometry designed for a TSR equal to 10. Hence, it can be concluded that the geometry corresponding to a TSR equal to 8 does perform better than the other geometry if they operate at their corresponding tip speed ratio.

Table 3.2: Comparison between the Blade Element Momentum (BEM) and the lifting line theory for the turbine.

	TSR=8		**TSR=10**	
	C_T	C_P	C_T	C_P
BEM	0.7500	0.4784	0.7500	0.4771
lifting line	0.7499	0.4807	0.7499	0.4780

3.2.2. Blade results

Next to the power coefficient and the thrust coefficient the effect of using the lifting line theory is also examined with respect to the flow distribution of the blades. Firstly, the radial distribution of the angle of attack is analysed, which can be seen in Figure 3.3. It can be seen both method give a similar angle of attack. However, it can be seen that close to the center of the rotor high angles of attack are experienced when simulated with the lifting line theory. Moreover, it can be seen that for both models the geometry with a TSR equal to 8 has a lower angle of attack at the root, whereas it has a higher angle of attack at the tip.

Next to the angle of attack, the radial distribution of the inflow angle is also computed and the result can be seen in Figure 3.4. Similar as for the angle of attack, it can be seen that the lifting line model estimates a similar inflow angle. As expected, the inflow angle also shows a significantly higher angle for the blade sections close to the root, induced by the relatively high angle of attack. Lastly, it can be observed that, in contrast to the angle of attack, both geometries do not have similar values for the inflow angle. Both geometries have a similar radial distribution, but the geometry optimised for a TSR equal to 8 is approximately 2 degrees higher than for the one designed for a TSR equal to 10.

Furthermore, the radial distribution of the bound circulation can be found in Figure 3.5. It can be seen that for the largest part of the radial distribution the lifting line method estimates a higher value for the circulation. This is not the

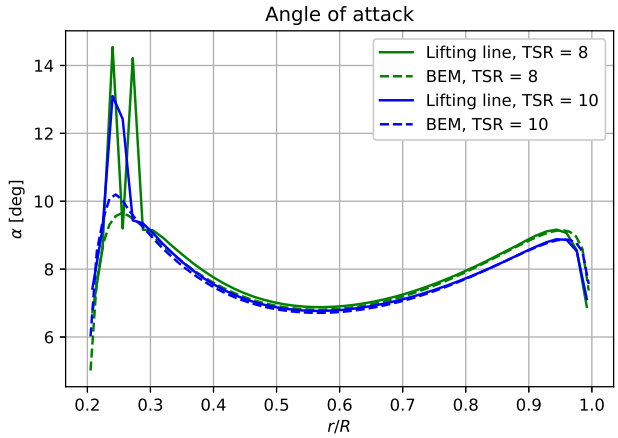

Figure 3.3: Radial distribution of the angle of attack for the turbine using BEM and the lifting line theory.

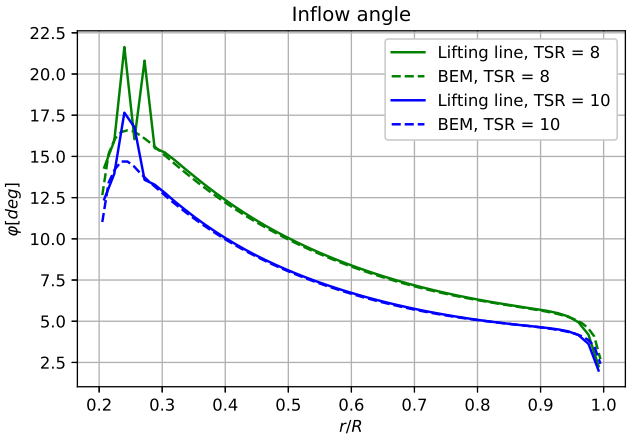

Figure 3.4: Radial distribution of the inflow angle for the turbine using BEM and the lifting line theory.

case for the blade elements close to the root, which is as expected as it is induced by the earlier observed significant difference for the inflow angle that the blade encounters. On top of that, it can be seen that the distribution for both models are almost equal for the two geometries and their tip speed ratios.

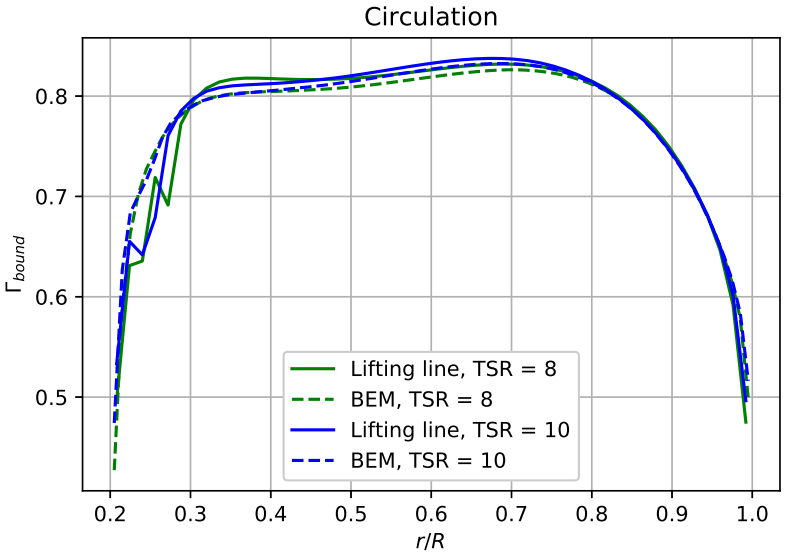

Figure 3.5: Radial distribution of the bound circulation for the turbine using BEM and the lifting line theory, non-dimensionalised by $\frac{U_\infty \pi}{N_{Blades}\Omega}$.

For the radial distribution of the circulation an analysis has also been done when an impermeability boundary condition is applied. The result of this analysis can be seen in Figure 3.6. In the legend of this figure "imper" corresponds to the result of the impermeability boundary condition, whereas "polar" corresponds to used model with the polar data provided by the course instructor. It can be seen that using the impermeability boundary condition results in a higher circulation near the root. This is probably due to the fact that this boundary condition assumes a linear relation between the angle of attack and the lift coefficient. On the other hand, the polar data shows that this is not true for higher angle of attacks as stall occurs. Using the observation that the inflow angle is relatively high close to the root shows that the circulation cannot be estimated to be a linear relation between the lift and the angle of attack. Hence, this should be taken into account when the impermeability boundary condition is used.

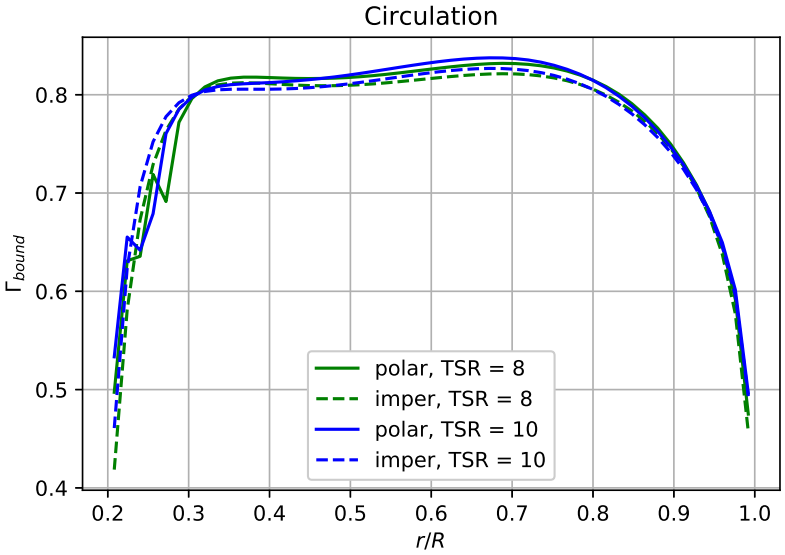

Figure 3.6: Radial distribution of the bound circulation for the turbine using the lifting line theory with different boundary conditions, non-dimensionalised by $\frac{U_\infty \pi}{N_{Blades}\Omega}$.

Furthermore, the tangential load was determined in order to obtain the power coefficient and the result can be seen in Figure 3.7a. Firstly, it can be observed that the geometry designed for a TSR of 8 experiences a higher tangential load than for the higher TSR case. This is as expected using the earlier made observation that the inflow angle is higher for the lower TSR case. Furthermore, it can be observed that the lifting line theory estimates a higher load than when BEM is used for the simulation. This was already shown with the observation in the previous section that the power coefficient is higher for the lifting line theory compared to BEM modelling. However, this difference is larger than expected as the difference in coefficient is not significant.

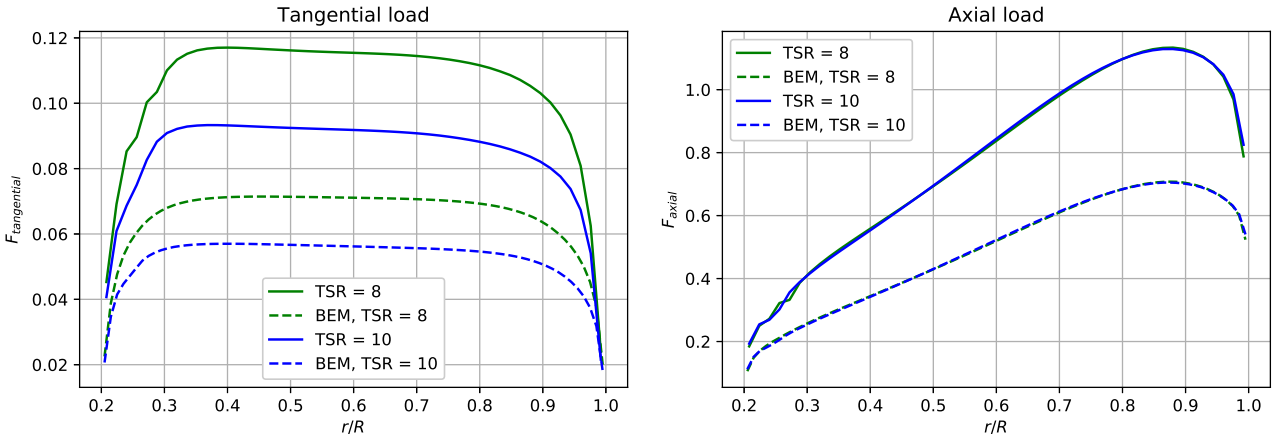

(a) Azimuthal load.

(b) Axial load.

Figure 3.7: Loads of a turbine blade normalized by $\frac{1}{2}\rho U_\infty^2 R$.

Next to the azimuthal load, the radial distribution of the axial load was also determined in order to determine the thrust coefficient of the turbine and this result can be found in Figure 3.7b. It can be observed that the simulation with the lifting line method again shows a higher value than for BEM despite the same value for the thrust coefficient. For future research this should be investigated. Moreover, it can be observed that for the lifting line method the axial load increases more in the direction from the root to the tip of the blade. Additionally, close to the root of the blade there is a discrepancy observed in the linear slope of the curve for the lifting line simulation. Again, an observation that can be explained with discrepancy in the inflow angle close to the root of the blades. Lastly, it can be seen that for both models the loads of the different geometries result in the same axial load, as expected using that they result in the same thrust coefficient.

4
Propeller

4.1. Geometry of the blade and vortex model

The analysis for the propeller uses the optimized geometry from an optimized blade element model (BEM), given in figure 4.1. The geometry was the result of a gradient descent optimization algorithm which optimizes each section of the blade individually.
As for the wake geometry, a frozen wake vortex model was used to describe the vortex. This method has a fixed shape, which is determined at the start of the simulation. The dimensionless length of the wake [N] is the result of the rotational speed and the wake velocity. Furthermore, the y and z axis represent the radial position.

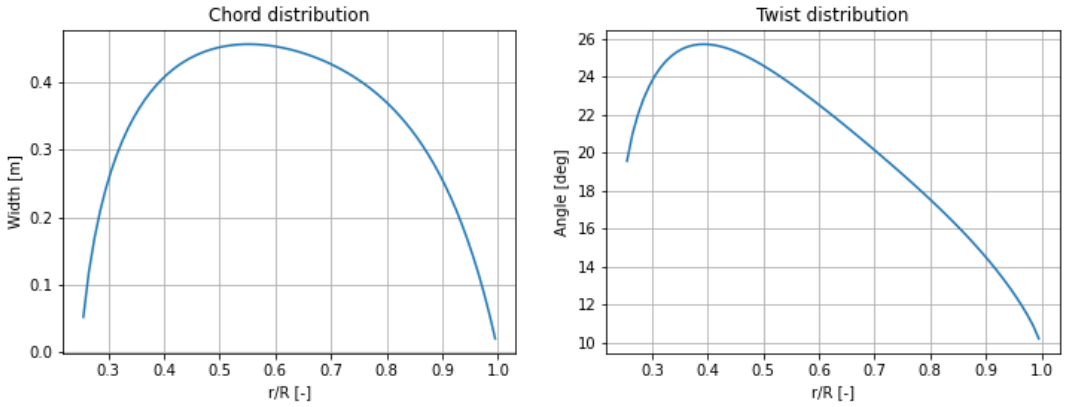

Figure 4.1: Chord distribution for the propeller.

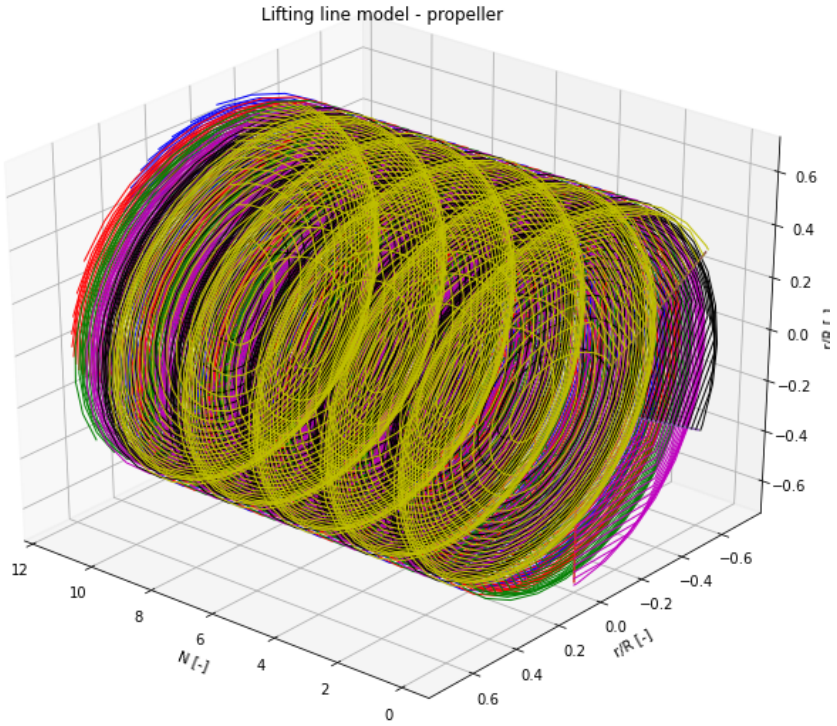

Figure 4.2: Visual representation of the model for the propeller.

4.2. Results

In this section the results for the lifting line analysis for the propeller are given. Each paragraph first discusses the results for the lifting line model individually and has a comparison with the blade element model. The analysis is only done for the propeller in energy harvesting condition. Firstly, the overall performance of the propeller are explained, followed by the blade properties.

4.2.1. General model results

The general results are explained in this paragraph.

There is one general remark about the BEM and lifting line model results. In the BEM model, the propeller blade was optimized for cruising speed. The polar C_L and C_D was defined for [-10° to 24.5°]. That resulted in the angle of attack in figure 4.3. This went well for the propelling scenario, for which most of the polar is defined. However, in the energy harvesting scenario, the inflow angles increases beyond the chord line and the angles of attack become negative. This is a problem since the polar is not defined for larger negative angles of attack than -10°. In our program, if the value went below -10°, the program would take the polar for -10°. Because of this, we believe that the results here are not realistic. Unfortunately, due to time constraints we were not able to solve this problem. Therefore, we will compare the results for the lifting line and the BEM model with this in mind.

Table 4.1: Power and thrust coefficients for a BEM model and lifting line model.

Analysis	C_T	C_P
BEM	0.622	0.384
Lifting Line	0.609	0.416

4.2.2. Blade properties

The flow properties, circulation and force coefficients per blade are explained in this paragraph. In every graph represents the orange line the lifting line results and the blue line the BEM results. The blade is uniformly discritized, similar to the blade in the BEM analysis.
The flow properties for each of the six blades are discussed here. The results are given in figure 4.3. The inflow angle follows a smooth curve starting at 63.1° and ending at 31.2°. The formula for the inflow angle is given in equation 4.1. As the radial position increases, the value for the $\omega \cdot r$ in the denominator increases, which decreases the inflow angle. That explains the decreasing smooth line for the lifting line case. The BEM inflow angle is more affected by the Prandtl tip and root correction, which increases the inflow angles at those locations.
The angle of attack is evaluated at the $\frac{1}{4}$ point of the chord. Figure 4.3 starts with the largest angle attack 44.9°, then follows an parabola shaped curve with a minimum of 14.4°, ending at a 20.7°. The shape of the curve is the result of the equation 4.2. The angle of attack is the difference between the inflow angle and the twist angle. At the tip of the blade in figure 4.1, the twist distribution declines faster than the inflow angle does, which results in an increasing angle of attack at that position. This explains the parabola shaped distribution of the angle of attack.

When comparing the inflow angles between the two methods used, BEM and lifting line, the latter has larger angles for all radial positions. On average, the difference is 30% with the maximum at 35% of the BEM value at r/R=0.33. One explanation for this difference is the different values for the axial induction factor, shown in figure 4.4. The relation between is the axial velocity, used for calculating the inflow angle and free stream velocity is $U_{axial} = U_\infty \cdot (1-a)$. The lifting line model has a lower axial induction factor than the BEM model, which increases the axial velocity and in turn the inflow angle.
When comparing both angles of attack, the angle of attack of the lifting line method is significantly higher than that of the BEM analysis. At the root of the blade, the difference quickly enlarges, to a maximum of 80% of the BEM value and remains at this difference. Only as it reaches the tip of the blade, the difference decreases.

$$\phi = \tan(\frac{U_{axial}}{\omega \cdot r}) \tag{4.1}$$

$$\alpha = \phi - \angle_{twist} \tag{4.2}$$

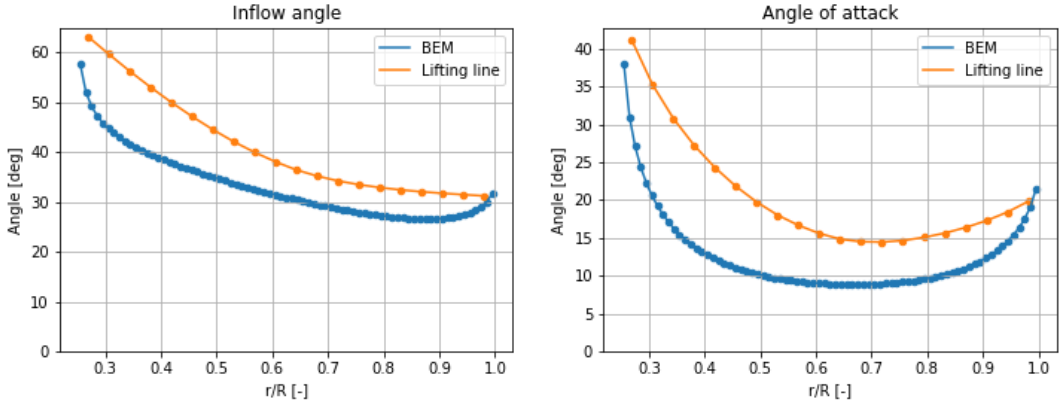

Figure 4.3: Angle of attack and inflow angle for the BEM and lifting line analysis.

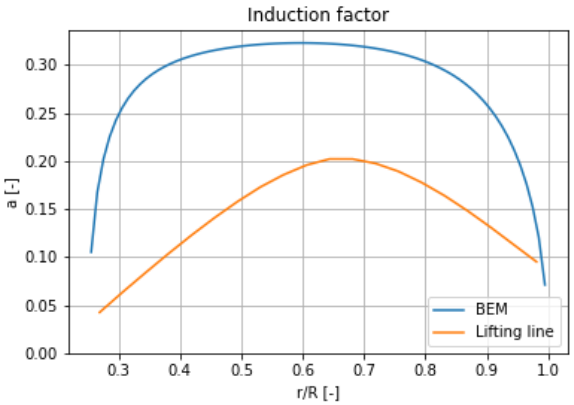

Figure 4.4: Induction factors for the lifting line method and BEM model.

The distributions for the circulations of both models is given in figure 4.5. The circulation for both models are very similar. There is a minor difference at the blade root, but after r/R-0.6 there is no difference between the two. This can be explained by the polar of the angle of attack, which is not defined for angles smaller than -10°. This is also explained in paragraph 4.2.1. In this model, the AoA is larger then the -10°, which means that the blade gives the same lift and drag coefficients for every radial position. This means that the circulation is also the same.

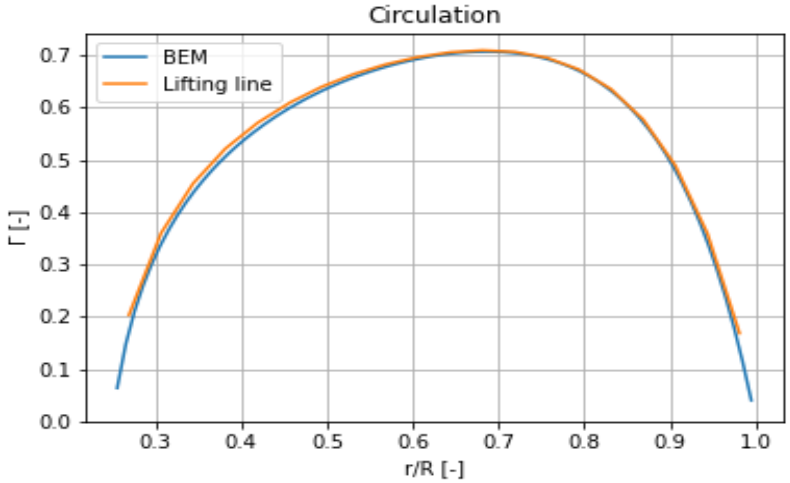

Figure 4.5: Circulation for the BEM and lifting line analysis. Normalized with $\frac{U_\infty^2 \cdot \pi}{\omega}$

The tangential and axial loads for one blade are given in figure 4.6. The non-dimensional tangential force shows an sharp increase near the blade root, followed by a smoothing of the curve until it reaches r/R=0.5. After this point, the

curve remains constant at 0.37. Finally, at r/R>0.75, the curve decreases sharply. The shape of this distribution can partly be explained by the formulas used and by the effect of the Prandtl tip and root correction. Firstly, the equation side. The lift and drag forces are calculated with equations 4.3 and 4.4. These values are used to find the tangential and axial forces on the blade section. The relationship is given in equations 4.5 and 4.6. The forces are influenced by the inflow angle ϕ. The smooth curve in figure 4.3 is translated in another smooth load figure. Secondly, the effect of the Prandtl tip and root correction decrease the tangential velocity of the blade. It corrects for the loss in efficiency due to root and tip vortices. The non-dimensional axial force shows a steady increase from the start with a maximum at r/R=0.78. After this point, the curve sharply decreases to the tip of the blade. One explanation for the sharp increase at the root and decrease at the blade tip is again the Prandtl correction applied. This results in lower lift and drag forces, which also affects the axial force exerted by the blade.

The difference between the BEM and the lifting line model can be explained in two ways. Firstly, in the BEM analysis, the force coefficients play a central role in the analysis while the circulation is a product of the forces on the blade. On the contrary to the lifting line, where the circulation is calculated and the tangential and axial forces are a product of the circulation on the blade. As the angles of attack are almost all above the -10°, they return the same lift coefficient, through which the circulation is calculated on the blade in the lifting line model. Thus, the circulation is the same as can be seen in figure 4.5. However, the inflow angles are very different and are used to calculate the tangential and axial force. Therefore, different values for the forces on the blade are found, while the circulation on the blade is the same. Basically, it is an error due to the lack of data in the polar files.

$$L = \frac{1}{2}\rho c r c_l U_r^2 \tag{4.3}$$

$$D = \frac{1}{2}\rho c r c_d U_r^2 \tag{4.4}$$

$$F_{tan} = L \cdot \sin(\phi) + D \cdot \cos(\phi) \tag{4.5}$$

$$F_{axial} = L \cdot \cos(\phi) - D \cdot \sin(\phi) \tag{4.6}$$

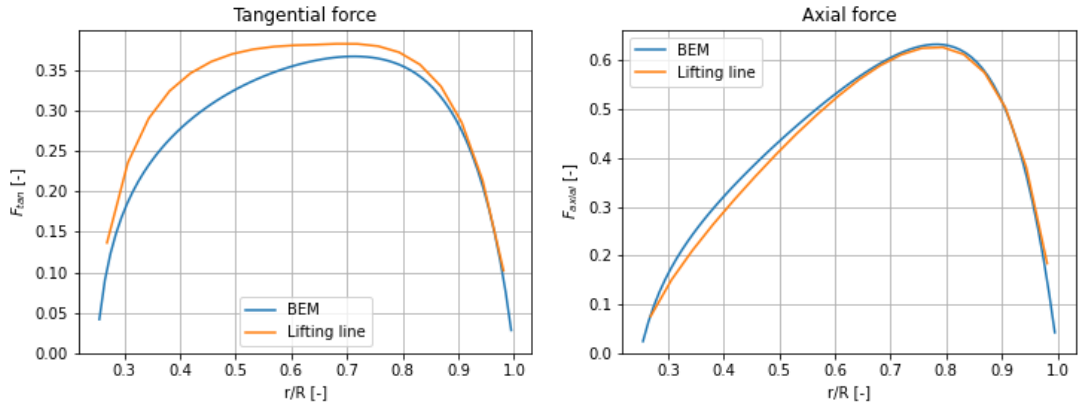

Figure 4.6: Tangential and axial force distribution for the BEM and lifting line analysis. Normalized with $\frac{1}{2} \cdot \rho \cdot R \cdot U_\infty^2$

5
Two Wind Turbines

In this chapter the effect of two wind turbines in the same plane on the turbine performance will be analysed in order to determine the effect of tip proximity of two rotors. First, the model and the analysis will be briefly discussed in Section 5.1. Afterwards, the results of the analysis will be presented in Section 5.2.

5.1. Model

The lifting line theory is used with the assumption of a frozen wake to analyse the performance of two of the exact same wind turbines in the same plane. The simulation parameters used for this are the same are presented in Table 5.1. Additionally, the performance will be analysed with varying distance between the rotor and phase difference between the two rotor axis of the turbines. The range of distances that were considered are presented in Equation 5.1, where $2R$ corresponds to the minimum distance between the two rotors as R equals the radius of the two rotors. The largest distance models corresponds to modelling a single turbine. Using this minimum distance would correspond to the wake geometry as can be observed Figure 5.1. Note, the analysis of the effect of distance on the performance is only for a tip speed ratio equal to 8.

$$L = [2R, 4R, 10R, 20R, 40R, 60R] \tag{5.1}$$

Parameter	Value
Number of blade sections	30
Number of wake sections	30
Number of rotations of the rotor	5
Wake convection induction factor a_{wake}	0.25
Vortex core size	0.25

Table 5.1: Parameters used for the lifting line model simulation for two turbine rotors.

Moreover, the range of phase differences considered are presented in Equation 5.2, where $\frac{2\pi}{3}$ is the maximum phase difference as the rotors have three blades. Again, this analysis is done for a tip speed ratio equal to 8.

$$\phi = \left[0, \frac{\pi}{3}, \frac{2\pi}{3}\right] \tag{5.2}$$

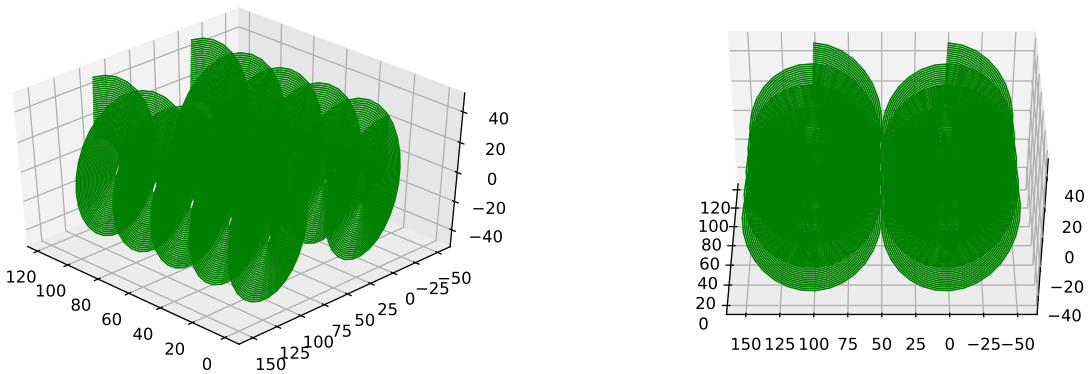

(a) Side view.

(b) Front view.

Figure 5.1: Visual representation of the wake of one of the blades of both turbines with zero phase difference and a tip speed ratio of 10.

5.2. Simulation results

The results that were obtained for two rotors in the same plane will be analysed in this section. For this the thrust and power coefficient are examined when there is no phase difference between the rotors and when both turbines correspond to the case with a tip speed ratio of 8. Afterwards, the other performance parameters and the flow distribution over the blades are analysed. This is followed by the effect of phase difference between the two turbines on the performance will be analysed. Lastly, the power coefficient is presented when the thrust coefficient equals 0.75 by altering the induction wake factor.

5.2.1. Thrust and power coefficient

Firstly, the thrust and power coefficient were determined and the result can be seen in Table 5.2. It can be seen that in case of two turbines that are positioned in the same plane result in a higher thrust and power coefficient than for two turbines that are positioned at a significant distance from each other. The effect of the distance on the power and thrust coefficient can be more visualised by observing Figure 5.2a and Figure 5.2b respectively. The effect of the distance between the two rotors on the coefficients seems to vary exponentially for a lower distance.

	TSR=8		**TSR=10**	
	C_T	C_P	C_T	C_P
Single turbine	0.7625	0.5009	0.7647	0.5051
Two turbines with a distance of $2R$	0.7692	0.5092	0.7712	0.5149
Two turbines with a distance of $4R$	0.7644	0.5039	0.7666	0.5079
Two turbines with a distance of $10R$	0.7627	0.5023	0.7648	0.5053
Two turbines with a distance of $60R$	0.7625	0.5009	0.7647	0.5051

Table 5.2: Comparison of the thrust and power coefficient for turbines in the same plane at different distances apart from each other.

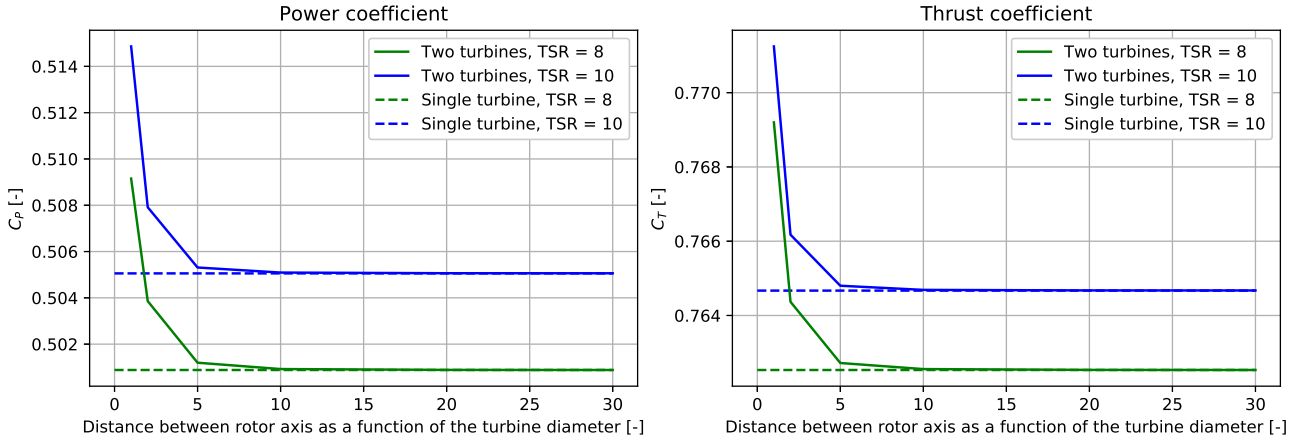

(a) Power coefficient

(b) Thrust coefficient

Figure 5.2: Power and thrust coefficient of a turbine rotor as a function of the distance between the rotor axis of two turbine rotor in the same plane.

5.2.2. Effect of distance between two rotors

First the effect of the distance between the two rotors is analysed regarding the circulation over one rotor blade. The result of the radial distribution of the circulation can be seen in Figure 5.3. Again, it can be seen that this increase in circulation for the largest part of the radial distribution decreases significantly if a rotor diameter is added to the distance. On top of that, it can also be observed that the higher angle of attack near the root results in a lower circulation, which could indicate that more lift loss is experienced because of a more forward flow separation.

Lastly, the loads are examined to observe the effect of the two turbine presence on the radial distribution of the loads. The azimuthal load and axial load variation can be observed in Figure 5.4a and Figure 5.4b respectively. It can be observed that the azimuthal load increases significantly if a second turbine is placed in the same plane at one diameter distance. On the contrary, it can be seen that the axial load does not differ significantly. This satisfies the earlier made observation regarding the thrust coefficient and the power coefficient. The power coefficient differs almost 1.7% between a single turbine and two turbines exactly next to each other, while this difference is 0.8% for the thrust coefficient. Taken into account that the azimuthal load and axial load are directly related to the thrust coefficient and power coefficient respectively, suggests a similar behaviour for adding another turbine in the same plane.

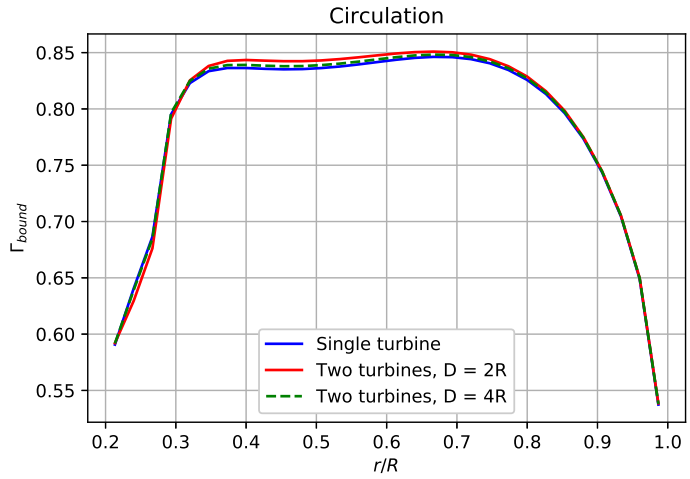

Figure 5.3: Circulation of a turbine blade as a function of the distance between the rotor axis of two turbine rotor in the same plane, for a TSR equal to 8.

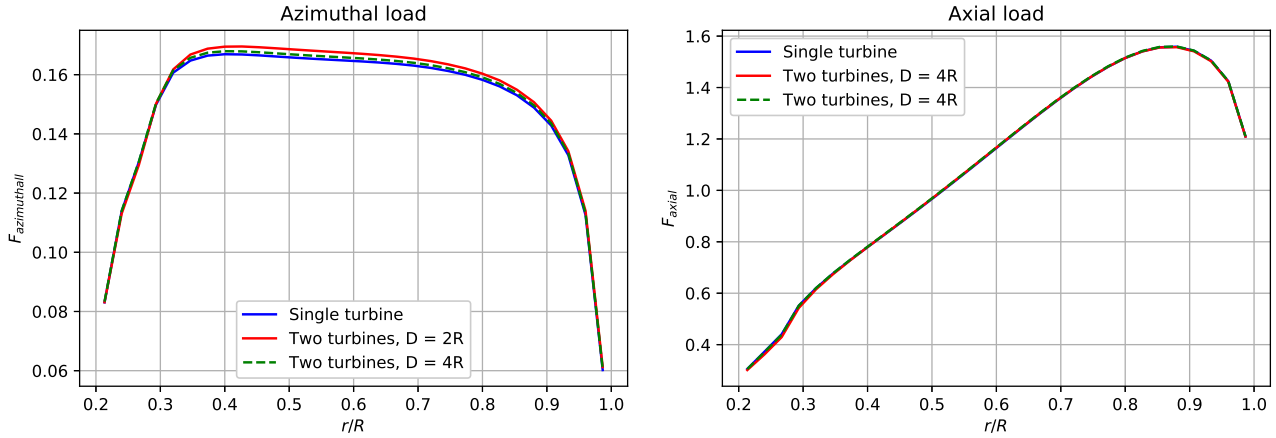

(a) Azimuthal load.

(b) Axial load.

Figure 5.4: Loads of a turbine blade as a function of the distance between the rotor axis of two turbine rotor in the same plane, for a TSR equal to 8.

5.2.3. Effect of phase difference between two rotors

In order to gain a complete overview of the performance of the turbine, the phase difference is also examined. This is done for the case with two turbines in the same plane with a diameter distance between the two rotor axis. The result can be found in Table 5.3 and visualised in Figure 5.5. It can be observed that any phase difference will result in a lower thrust and power coefficient of the turbine and hence the turbine will operate with a lower efficiency. Moreover, it can be observed that the effect of phase difference is higher for the higher tip speed ratio.

Table 5.3: Comparison of the thrust and power coefficient for turbines in the same plane at different distances apart from each other.

	TSR=8				**TSR=10**			
	C_T	Δ	C_P	Δ	C_T	Δ	C_P	Δ
$\phi = \mathbf{0}$	0.7692	0.0%	0.5092	0.0%	0.7712	0.0%	0.5149	0.0%
$\phi = \frac{\pi}{3}$	0.7686	-0.08%	0.5080	-0.24%	0.7708	-0.05%	0.5140	-0.17%
$\phi = \frac{2\pi}{3}$	0.7692	0.0%	0.5092	0.0%	0.7712	0.0%	0.5149	0.0%

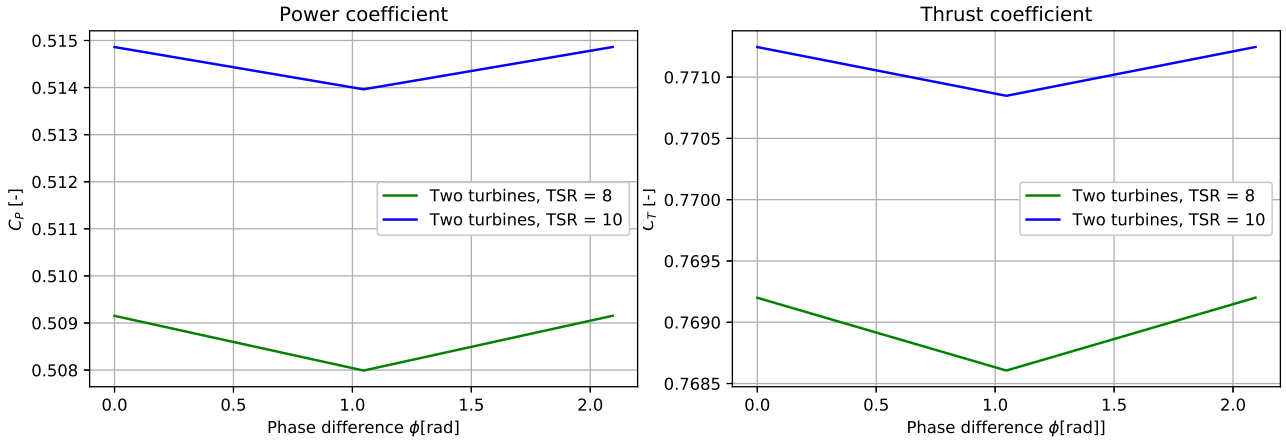

(a) Power coefficient

(b) Thrust coefficient

Figure 5.5: Power and thrust coefficient of a turbine rotor as a function of the phase difference between the two turbine rotors with one diameter distance between the two axis.

As can be seen in Table 5.3, the differences is relatively small and thus difficult to observe in the radial distribution of the performance parameters. Nevertheless, the effect can be observed in the radial distribution of the inflow angle. As can be observed in Figure 5.6 the inflow angle decreases when a phase difference occurs.

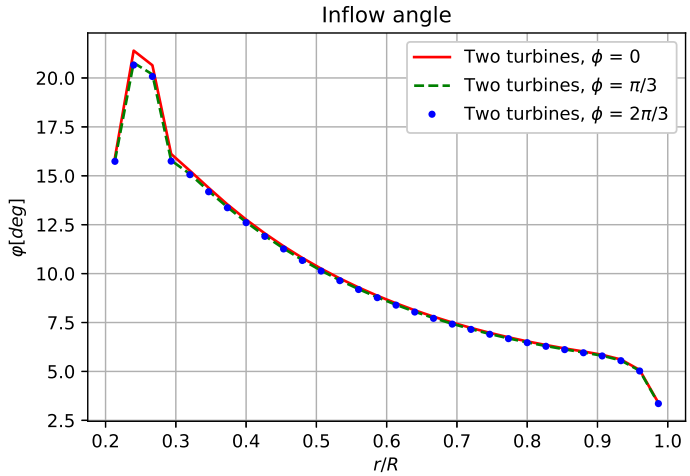

Figure 5.6: Circulation of a turbine blade as a function of the distance between the rotor axis of two turbine rotor in the same plane, for a TSR equal to 8.

All in all, it can be concluded that two turbines in the same plane at a distance close enough will result in an increase of the thrust and power coefficient. However, this is for a simulation with the same wake induction factor for the single and two turbines. For future research, it should be investigated what the difference in this wake induction factor is. It is expected that two turbines close to each will result in a lower convection speed of the wake as the wake of one turbine will slow down the inflow speed of the other turbine, resulting in a wake close to both turbines. Moreover, it should be aimed to have a zero phase difference in order to achieve the highest thrust and power coefficient.

6
Conclusion

In this report, the lifting line model was evaluated for three situations: one turbine, one propeller and two turbines perpendicular to each other. A frozen wake was assumed. Furthermore, the single rotor cases were compared to the results of the BEM analysis of the previous assignment.

The analysis made it able to draw several conclusions. First of all, In the sensitivity analysis, the effect of wake convection speed, spatial discretization, viscous core size and wake length were analyzed. Based on the results, the best settings for rest of the assignment were determined. The wake convection speed and the wake length were most influential on the results for the turbine. The viscous core size turned out to be important for the smoothness of the circulation over the blade. Finally, the spatial discretization are important, especially for the root and the tip of the blade. Besides the effect on the performance, also execution time was taken into account. Especially in the determination of the optimum wake length and number of blade section, it was influential. There the trade off between the two was clear and the best settings were determined.

Secondly, the propeller results for the lifting line were discussed and compared to the results of BEM model. The major discovery was the lack of data on the polars. The angle of attack for the propeller was larger than -10° while the polar was defined untill -10°. The program was designed such that it would take the C_L and C_D which would correspond to the minimum defined angle of attack and not interpolate to the actual angle of attack. This distorted the results severely, since the blade geometry optimizatio in the BEM analysis was done in a similar way. Nevertheless, there were some differences between the lifting line and the BEM analysis. Firstly, the lifting line model resulted in larger angles of attack than the BEM model. However, the circulation remained the same, which resulted very different tangential and axial loads.

Regarding the wind turbine it was shown that the lifting line method resulted in a higher estimation of the power coefficient for a similar thrust coefficient, than was computed for the blade element momentum theory as done in the previous assignment. This higher estimation was also shown in the radial distribution of the angle of attack, inflow angle, circulation. However, for both the axial and the tangential load it was shown that the lifting line method resulted in a significant higher estimation of these loads. Additionally, the use impermeability boundary conditions showed a lower accuracy of the results as these did not take stall into account and assumed a linear relation between the alpha of attack and lift coefficient for high angle of attacks as well.

Moreover, the effect of two rotors in the same plane has been analysed. This was done by simulating two turbine rotors in the same plan with different distances between each other. It was shown that two turbine rotors close to each other in the same plan resulted in a higher power and thrust coefficient. Hence, it can be concluded that the efficiency increased. It was observed that this positive effect degrades exponentially for an increasing distance. Next to this, the effect of the phase difference between the two rotors was analysed for the minimum distance between both turbines. It was shown that a phase difference results in a lower power and thrust coefficient of the turbines. Hence, this effect should be taken into account when a maximum efficiency of the turbine is wanted. For the simulation the same wake convection factor was taken. However, in real life it is expected that this factor is lower for the two turbine case. In real life it is expected that the induction convection speed is lower for two turbines with interfering wakes. And hence the induction wake factor is expected to be higher than for the single rotor case, resulting in a lower power coefficient and thrust coefficient subsequently. For future research it is recommended to first test and develop a model to determine the difference in the wake convection speed for the two cases.

Bibliography

[1] E.M. Greitzer, C.S. Tan, and M.B. Graf. *Internal Flow: Concepts and Applications*. Cambridge Engine Technology Series. Cambridge University Press, 2007.

[2] John Anderson. *Fundamentals of Aerodynamics*. McGraw-Hill Education, United States of America, 2017.